1.D.1:
1.D.2

Nuclear Physics **A183** (1972) 257—284; © *North-Holland Publishing Co., Amsterdam*

CORIOLIS EFFECTS IN THE YRAST STATES

F. S. STEPHENS † and R. S. SIMON
Sektion Physik, Universität München, München, Germany ††

Received 19 November 1971

Abstract: We have investigated the Coriolis effects at high angular momentum in a system consisting of two (or four) particles in the $i_{\frac{13}{2}}$ orbital coupled to a deformed core. As the angular momentum is increased in this system, we find that the particles tend to decouple from the core and add their angular momenta, ultimately $2j-1$ for two particles, directly to that produced by the rotation of the core. In our calculations, enough energy is gained in this partial decoupling so that somewhere between $I = 10$ and $I = 20$ these states become lower in energy than those involving just rotation of the initial system. Such a change in the character of the lowest-lying, or yrast, level in this spin region is consistent, in so far as we can tell, with existing experimental data on rotational-level spacings and de-excitation cascades.

1. Introduction

For a given angular momentum, the state of lowest energy in a nucleus is called the yrast state. For angular momenta lower than about 10 $\hbar$, these states are reasonably well known and understood in most nuclei, but there is much less information about yrast states of considerably higher angular momentum. A systematic way to populate such states is to bombard various target nuclei with heavy ions under conditions where compound-nucleus formation occurs – the (HI, xn) reaction. If, for example, the target nuclei are chosen in the region of Sn ($Z = 50$) and projectiles such as Ar ($Z = 18$) are used, whose energy is slightly above the Coulomb barrier, then rare-earth product nuclei are formed, after the evaporation of several neutrons, having excitation energies $\approx$ 20 MeV and angular momenta up to 40–50 $\hbar$. The γ-ray cascades de-exciting these nuclei have provided much of the available information about high-spin yrast states. This information has recently been summarized and some of its implications about the nature of such high-spin states discussed [1]). We will briefly review this discussion, since the present work was motivated mainly by the desire for a better understanding of this de-excitation process.

The γ-ray spectrum from product nuclei of the type mentioned above almost invariably consists of a set of discrete lines on a continuous background. In rotational and vibrational nuclei the lines correspond to the transitions in the ground state col-

† On leave from Lawrence Berkeley Laboratory, University of California, Berkeley, California (present address: Lawrence Berkeley Laboratory, University of California, Berkeley, California 94720).

†† This work was partially supported by the US Atomic Energy Commission.

lective band (g.s.b.) †, and represent the last steps of the de-excitation. Thus the γ-ray transitions between the high-spin states are in the continuous background. Up to now very few direct studies of this continuum have been made, so that the information about the high-spin states is based on observations of the transitions between lower-spin states, i.e. the discrete lines. The following points, made in ref. [1]), are relevant to the present work: (a) the maximum spin observed in the g.s.b. ranges from around 16 for rotors to around 6 for vibrators, and this maximum is characteristic of the particular nucleus (not of the reaction); (b) however, when heavy ions are used to produce the compound nucleus (bringing in high angular momentum) then the g.s.b. is fed *mostly* at or near the highest observed level, whereas with light projectiles the feeding pattern is related to the distribution of angular momentum brought in by the projectile; (c) the mean time interval between the reaction and population of the g.s.b. in rotational nuclei is very short, $\lesssim$ 10 psec; and (d) very high-spin isomers, $I \gtrsim 20\ \hbar$, have never been observed. It should be emphasized that these are features observed in (especially) rotational and vibrational nuclei, and would not apply, without modification or qualification, to closed-shell or near-closed-shell nuclei.

To understand these four points, the de-excitation was described in ref. [1]) as consisting of three cascades, whose existence had been previously proposed by Grover [2]) based on numerical studies of the process. Since the initial energy (20 MeV) and level density are high, a statistical cascade (I) consisting mainly of high-energy dipole transitions is expected to occur first. This carries off around half the excitation energy but very little angular momentum and is terminated by coming into a region where the level density is no longer high. This region is located just above the yrast level and would be $\approx$ 10 MeV for $I \approx 35$ in the above example. At this point the cascade is forced to begin carrying off angular momentum and follows, more or less closely, the yrast levels down in spin. This is called the yrast cascade (II). At some spin the yrast levels become those of the g.s.b. and an energy gap develops between these levels and others of the same spin. At this point the population shifts rather suddenly into the g.s.b. through which it cascades (III) to the ground state. Fig. 1, which is taken from ref. [1]) shows the essential features of these three cascades. For lighter projectiles, where less angular momentum is brought in, the length of the yrast cascade shortens, until it is essentially absent in reactions induced by ^{4}He.

Two interesting conclusions were drawn in ref. [1]) about this de-excitation. First, the very short feeding times (c) and absence of isomeric states with high spin (d) indicate that energies in the high-spin yrast region must be very smooth and the transitions between these levels must be enhanced over the single-particle value if they are E2. (Other choices for the predominant multipolarity turn out to be much more difficult to explain.) Furthermore, to avoid the generation of discrete lines in this region, the population must be spread over several ($\gtrsim$ 5) levels. It was suggested [1]) that the

† The g.s.b. refers to the collective band based on the ground state configuration of a particular nucleus. For the doubly even nuclei considered here, this is a completely paired configuration (zero quasi-particles) and the levels of this band are the yrast levels at low spin values.

presence of rotational bands admixed by the strong Coriolis force present at these high spins might produce such features. Mottelson [3]) has pointed out that the spectrum of an asymmetric rotor is a particularly simple one fulfilling these requirements of the yrast cascade, but a model for the de-excitation based on this suggestion has not been published. The second conclusion of ref. [1]) was that the feeding point of the g.s.b. was near its intersection with other levels. No other way could be found to explain the population patterns. This intersection implies a major change in the nature of the

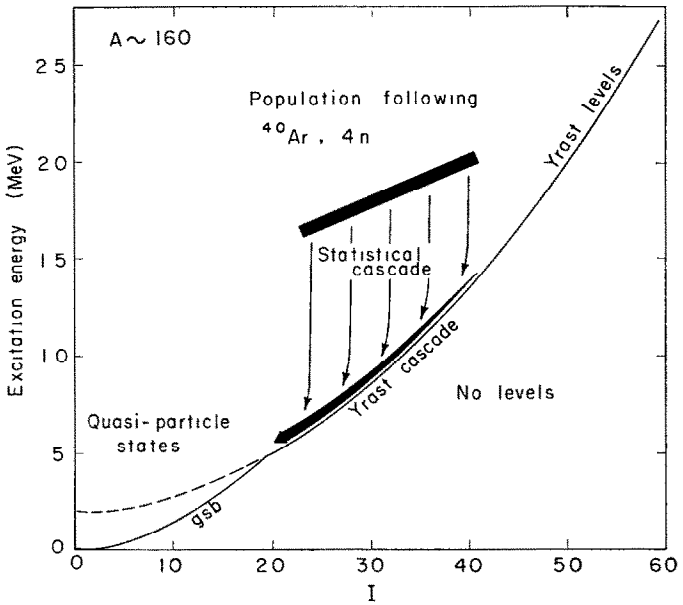

Fig. 1. Excitation energy is plotted against angular momentum in a nucleus (with mass around 160) that is the product of an (^{40}Ar, 4n) reaction. The populated energy and angular momentum range is shown, together with the proposed cascade pathway to the ground state.

yrast levels above this spin value, and it was suggested in ref. [1]) that this might be related to changes in the pairing correlations of the nucleus.

Very recently Johnson *et al.* [4]) have found some irregularities in the rotational energy spacings of rare-earth nuclei just in the region of spin where they are populated heavily in these (HI, *x*n) reactions. It is too early to say how general this behaviour is, but it lends very strong support to the previous proposal that a major change is occurring in the yrast levels near this point. Johnson *et al.* suggest that this change is due to the phase transition associated with the loss of pairing correlations predicted by Mottelson and Valatin [5]) to occur at around this spin value.

From the above discussion one can conclude that there is good evidence for a major change in the nature of the yrast levels of rare-earth nuclei somewhat below $I = 20$, and furthermore, that at higher spin values a new very regular structure develops. If

we confine ourselves to rotational nuclei, both because most of the above data relate to this type and because they are considerably easier to understand, then it seems reasonably clear that the primary new features at high angular momentum are the presence of strong centrifugal and Coriolis forces. There is experimental evidence [6]) that in good rotors such as ^{154}Sm the centrifugal stretching up to spin 8 is very small, if it occurs at all. Although the stretching may well be appreciable for larger spins, it seems unlikely to cause the major effects described above. On the other hand, any simple estimate indicates that the Coriolis effects can be very large, and furthermore, they are known to be involved in determining the yrast levels at rather low spins ($I \approx 10$) in some odd-mass rare-earth isotopes [7]). We have therefore attempted to evaluate the direct effects of the Coriolis force on the nuclear levels. By direct effects we mean those that result from the diagonalization of the Coriolis interaction among a given set of levels. This simple procedure does not take into account changes due to other types of interaction (centrifugal stretching, for example) nor more subtle effects of the Coriolis force itself (the Mottelson-Valatin effect, for example). This while we cannot expect all the changes occurring in nuclei at high spins to be direct Coriolis effects, we can expect such effects to provide a background which *is* occurring and against which other changes might be identified. It seems to us useful, and perhaps even essential, to understand this background.

2. Framework for the calculations

In order to calculate the direct Coriolis effects in doubly even nuclei, we must first decide which states must be included in the calculation and which can be omitted. This is essential since there are otherwise a virtually unlimited number of two-, four-, etc., quasiparticle states to consider. Fortunately, it turns out to be rather straightforward to select the important states; namely the ones that lie low in energy and have large Coriolis interactions. As far as the energy is concerned, one can say that the 2-quasiparticle (2-q.p.) states lie lowest, after the ground band (0-q.p.), then the 4-q.p. states, etc., and apart from this it depends on the exact location of the Fermi surface. The requirement for large Coriolis interactions is much more specific. The Coriolis matrix elements are

$$H_C = -\frac{\hbar^2}{2\mathscr{I}} \langle \Omega \pm 1 | j_\pm | \Omega \rangle \sqrt{(I \mp K)(I \pm K + 1)} f(U, V), \tag{1}$$

where $\mathscr{I}$ is the moment of inertia, $f(U, V)$ is a reduction factor due to the pairing which is defined later, and the matrix element, $\langle \Omega \pm 1 | j_\pm | \Omega \rangle$, contains the dependence of H_C on the particle state, Ω. The value of $\langle \Omega \pm 1 | j_\pm | \Omega \rangle$ can be calculated from a given set of particle wave functions, for example, those of Nilsson [8]), and an examination of these values is instructive. For neutrons in the 82–126 shell, the states based on the $i_{\frac{13}{2}}$ orbital have a value (for a deformation $\beta = 0.3$) of 5.5 when one averages over all Ω-values; whereas, the remaining states in this shell have an average of only

1.1. The reason for this is well known to be that the value of this matrix element depends on the value of j (if j is a good quantum number, this matrix element just has the value, $\sqrt{(j\mp\Omega)(j\pm\Omega+1)}$). Not only is this large initially for the states from the $i_{13/2}$ orbital, but it remains large with increasing deformation since there are no nearby positive-parity states with which to mix. Thus, for these states, j *is* approximately a good quantum number, $\frac{13}{2}$. For the negative-parity states in this shell, however, j is both smaller initially and further reduced by the mixing of j-values caused by the deformation. One might think that either due to the larger number of negative-parity states or by picking out the few having the largest values of $\langle\Omega\pm1|j_\pm|\Omega\rangle$, this disadvantage in the average value might be overcome. However, in these cases the average energy separation between states connected by an appreciable Coriolis matrix element is higher than for the $i_{13/2}$ states, and the Coriolis effects remain weaker. The importance of this large advantage of the $i_{13/2}$ states over the others in this shell can be appreciated by considering eq. (1) and noting that for large values of I, $\sqrt{(I\mp K)(I\pm K+1)}$ is approximately equal to I. Therefore, in a particular nucleus the value of I at which a given value of H_C is reached is inversely proportional to $\langle\Omega\pm1|j_\pm|\Omega\rangle$, or on the average a factor of 5 lower for the $i_{13/2}$ states than for the negative-parity states in this shell. Thus, with increasing spin, the major Coriolis effects should happen much earlier for the $i_{13/2}$ states. This suggests that it might be reasonable to consider the Coriolis effects among the states from the $i_{13/2}$ orbital explicitly, and to assume that the other states form an inert core that only rotates. This is the model we have chosen to explore.

A situation rather similar to the one described above also occurs in the 50–82 proton shell, where the $h_{11/2}$ orbital plays the same role as the $i_{13/2}$ above. However, Coriolis effects in the component states of the $h_{11/2}$ orbital are smaller than in those of the $i_{13/2}$ one, not so much because of the lower average value of $\langle\Omega\pm1|j_\pm|\Omega\rangle$, 4.7 cf. 5.5, but because the $h_{11/2}$ proton shell is filled to a greater extent when the deformation sets in around $N = 90$ and $Z = 60$. This filling means two things: first, that near the Fermi surface the energy separation between states connected by Coriolis matrix elements will be larger since it increases sharply with Ω; and second, that the low-Ω states, which turn out to be extremely important, lie much higher in the quasiparticle spectrum. The importance of the high-j orbitals in Coriolis effects and the greater importance of $i_{13/2}$ neutrons relative to $h_{11/2}$ protons is well verified experimentally in the light rare-earth region. The exceptionally large moments of inertia observed for these states are basically due to these large Coriolis matrix elements, the ground band in ^{161}Dy being an outstanding example, with that in ^{165}Ho large, but not so outstanding. Also the tendency for these states to occur at relatively low energies for moderately high spin values, due to the heavy Coriolis mixing, is quite pronounced in the one-quasiparticle spectrum of the light Er and Dy nuclei [7]), and is also observed, but is less dramatic, for the light Ho isotopes [9]). Thus it seems safe to conclude that the Coriolis effects in the rare-earth region will be largest in states based on the $i_{13/2}$ neutron orbital.

For rare-earth nuclei, then, we want to evaluate the direct Coriolis effects in 2-q.p. levels based on the $i_{13/2}$ neutron orbital. If we consider a situation where the Fermi sur-

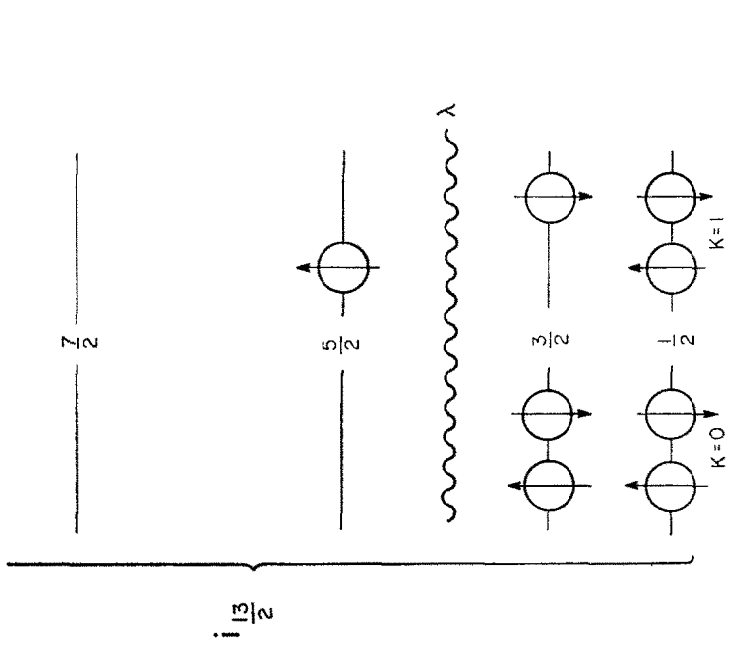

Fig. 2. Placement of particles in the states based on the $i_{\frac{13}{2}}$ orbital in a doubly even nucleus with a Fermi surface, λ. The left side of the figure represents the most probable situation for the ground state, whereas the right side shows a low-lying two-quasiparticle state. Many levels from other orbitals would be intermixed with these, but for simplicity are not shown.

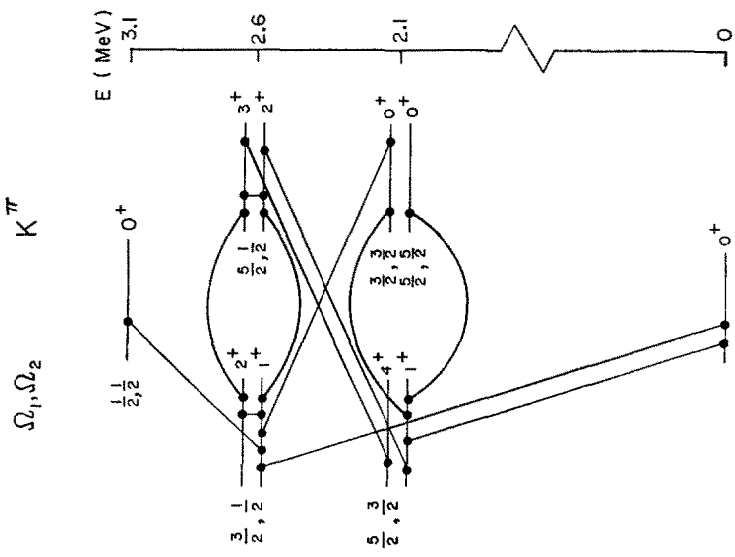

Fig. 3. The ten states possible considering only 2-q.p. states in the $\Omega = \frac{1}{2}$, $\frac{3}{2}$ and $\frac{5}{2}$ components of the $i_{\frac{13}{2}}$ orbital plus the ground state (0-q.p.). The interconnecting lines show the locations of non-zero Coriolis matrix elements.

face, λ, is between the $\frac{3}{2}$ and $\frac{5}{2}$ states of this orbital (corresponding to about 94 neutrons), then the left side of fig. 2 represents the most probable situation in the ground state of a doubly even nucleus. The particles are paired and occupying the lowest available states, though they would be frequently scattered into other states by the pairing force. The right side of fig. 2 shows one of the lowest 2-q.p. states of the type we want to consider, both quasiparticles in the $i_{\frac{13}{2}}$ states, and this state is connected with the ground state by a Coriolis matrix element of the type given in eq. (1). We can then move these two particles around among the $i_{\frac{13}{2}}$ states and generate many more 2-q.p. states. As an example, we show in fig. 3 the ten states possible if we limit the $i_{\frac{13}{2}}$ states to those having $\Omega = \frac{1}{2}, \frac{3}{2}$ and $\frac{5}{2}$. The lines interconnecting some of these states show all the possible Coriolis matrix elements. The energies of the 2-q.p. levels were taken to be

$$E_K(I) = E_{\nu 1} + E_{\nu 2} + \frac{\hbar^2}{2\mathscr{I}}[I(I+1) - K^2], \tag{2}$$

where

$$E_\nu = \sqrt{(\varepsilon_\nu - \lambda)^2 + \Delta^2}, \tag{3}$$

with ε_ν indicating the Nilsson eigenvalue at $\eta = 6$, λ the Fermi surface, and 2Δ the energy gap due to the pairing correlations. The Coriolis matrix elements are taken from eq. (1) where

$$f(U, V) = \begin{cases} (U_1 U_2 + V_1 V_2) \begin{cases} 2\text{q.p.} - 2\text{q.p.} \\ 4\text{q.p.} - 4\text{q.p.} \end{cases} \\ (U_1 V_2 - V_1 U_2) \begin{cases} 0\text{q.p.} - 2\text{q.p.} \\ 2\text{q.p.} - 4\text{q.p.} \end{cases} \end{cases} \tag{4}$$

The U and V coefficients are given by

$$V_\nu^2 = \frac{1}{2}\left(1 - \frac{\varepsilon_\nu - \lambda}{E_\nu}\right),$$
$$U_\nu^2 = 1 - V_\nu^2. \tag{5}$$

When a set of levels and matrix elements such as indicated in fig. 3 has been generated for a given I, it can be diagonalized, and the solutions give the Coriolis-mixed states for that I.

3. Physical model

Before discussing the results of the calculation it is useful to try to understand the physical process occurring. This is not only to give insight into the process but also to provide a basis for interpreting the wave functions that are produced. We begin by considering the Coriolis effects in a simple macroscopic system – a spinning wheel constrained to turn with a turntable. Fig. 4a represents this situation. The Coriolis effects in this system manifest themselves as a force tending to align the axis of the

wheel with that of the turntable in such a way that the direction of rotation is the same in both. This arrangement is indicated in fig. 4b. The relevance of this simple system to our nuclear model is as follows. The spinning wheel represents an $i_{\frac{13}{2}}$ particle and the turntable represents the rotating deformed core. If we consider a prolate core, then the symmetry (long) axis lies in the plane of the turntable and the turntable is just this core rotating about an axis (vertical in fig. 4a) that is perpendicular to its symmetry axis. Initially the $i_{\frac{13}{2}}$ particle is bound to the core in some way prescribed by the usual forces in the absence of rotation (fig. 4a), but as the nucleus rotates, the Coriolis force tries to decouple it from the core and align it as shown in fig. 4b. This decoupling process is well known for $K = \frac{1}{2}$ bands and, in the case of a single particle

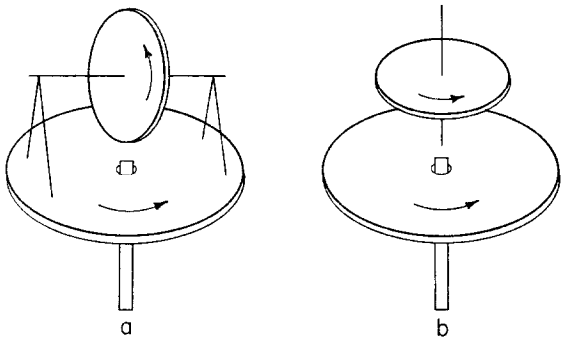

Fig. 4. The Coriolis effects on a spinning wheel constrained to turn with a turntable (a) tend to produce the configuration shown in (b).

in the $i_{\frac{13}{2}}$ orbital, it has been discussed by Vogel [10]). When two particles are considered, both tend to decouple in this way, producing the maximum possible angular momentum oriented as in fig. 4b. It is easy to see that the decoupling costs the nucleus something, since the configuration implied by fig. 4b is neither axially symmetric nor consistent with the pairing correlations, the latter of which requires the particles to couple to zero angular momentum. Our calculations represent an estimate of what compromise the nucleus makes between the structure preferred by the nuclear forces in the absence of rotation (expressed by the input spectrum) and that preferred by the Coriolis force.

The relevant coupling scheme is shown in fig. 5. Here the z-axis represents the symmetry axis of the nucleus and the angular momentum of its rotation is given by R. The two $i_{\frac{13}{2}}$ particles with projections Ω_1 and Ω_2 on the symmetry axis couple to give J with projection K, which in turn is coupled with R to give the total angular momentum of the system, I, and its projection, K. To describe the system represented in fig. 4b is just a matter of coupling the two j-vectors parallel to R; that is, in such a way as to give the maximum possible I. Following the scheme of fig. 5, this is accomplished by coupling the two $i_{\frac{13}{2}}$ particles to a J of 12, and then this to an R or $I-12$ to give I. Below $I = 12$ the prediction from fig. 4b is not so obvious. The general expression for

coupling these three vectors with a good intermediate J-value is

$$|(jj)J, R; IM\rangle \equiv |(JR)IM\rangle$$
$$= \sqrt{\frac{2R+1}{8\pi^2}} \sum_{\Omega_1, \Omega_2, K} \langle j\Omega_1 j\Omega_2 | jjJK\rangle \langle JKR0|JRIK\rangle |j\Omega_1\rangle |j\Omega_2\rangle \mathscr{D}^I_{MK}, \quad (6)$$

where the quantities in brackets are Clebsch-Gordan coefficients, and the D-function is the usual rotational wave function. The states, $|j\Omega\rangle$, have a good j-value, and for the $i_{13/2}$ components we are interested in, this is probably a rather good approximation.

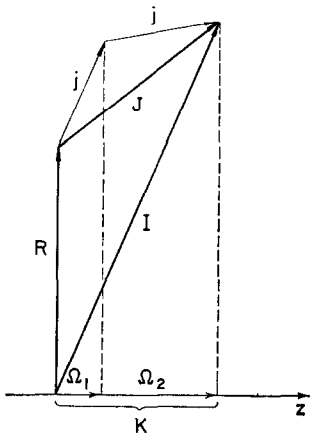

Fig. 5. The coupling scheme discussed in the text. It should not be inferred from this sketch that all these quantities have sharp values simultaneously.

However, a Nilsson wave function, for example, could be used, involving a sum over j-values. For the particular coupling discussed above, eq. (6) becomes

$$|(12, I-12)IM\rangle = \sqrt{\frac{2R+1}{8\pi^2}} \sum_{\Omega_1, \Omega_2, K} \langle \tfrac{13}{2}\Omega_1 \tfrac{13}{2}\Omega_2 | \tfrac{13}{2}\tfrac{13}{2}12K\rangle$$
$$\times \langle 12KI-120|12I-12IK\rangle |\tfrac{13}{2}\Omega_1\rangle |\tfrac{13}{2}\Omega_2\rangle \mathscr{D}^I_{MK}. \quad (7)$$

The usefulness of this is that we can form the overlap of eq. (7) with the solutions from our model and see the extent to which a given state corresponds to that represented by fig. 4b, or to any other configuration with a good J and R. Thus we can get some idea of the physical meaning of the solutions.

It is now interesting to consider the limiting case of complete decoupling for the 2-q.p. states, which is what Vogel [10]) did for the one-particle case. The lowest level, of course, is the one illustrated in fig. 4b, but we would like an estimate of the energy of this level as well as that of other levels. On the assumption that the core is axially

symmetric, the hamiltonian of the system we are considering can be written

$$H = H_{\text{intr}} + H_{\text{rot}} = H_{\text{intr}} + \frac{\hbar^2 \boldsymbol{R}^2}{2\mathscr{I}}, \tag{8}$$

where H_{intr} describes the coupling of the two $i_{\frac{13}{2}}$ particles to the core and to each other. However, the essential point of complete decoupling is that the orientation of the particles is independent of that of the core and each other. Thus, for this case, H_{intr} is a constant, and from eq. (8) we can obtain

$$E(I) = E_0 + \frac{\hbar^2}{2\mathscr{I}} R(R+1), \tag{9}$$

where R can take on values 0, 2, 4, . . . and J can have any value consistent with the coupling scheme, which requires

$$\boldsymbol{I} = \boldsymbol{R} + \boldsymbol{J}. \tag{10}$$

The energy, E_0, required to decouple the particles from the core is not so easy to estimate, but it must be in excess of 2Δ, the energy required to remove the two particles from the pairing correlations.

The relationship of this simple spectrum to the ones we obtain from diagonalization can be better understood if we rewrite eq. (8) in the more familiar coupling scheme. Combining eqs. (8) and (10) gives

$$H_{\text{intr}} + \frac{\hbar^2 \boldsymbol{R}^2}{2\mathscr{I}} = H_{\text{intr}} + \frac{\hbar^2 [\boldsymbol{I}-\boldsymbol{J}]^2}{2\mathscr{I}} = H_{\text{intr}} + \frac{\hbar^2}{2\mathscr{I}} [\boldsymbol{I}^2 - 2\boldsymbol{I}\cdot\boldsymbol{J} + \boldsymbol{J}^2]. \tag{11}$$

Using the facts that $\boldsymbol{I}^2 = I(I+1)$ and $\boldsymbol{J} = \boldsymbol{j}+\boldsymbol{j}$ and $I_z = J_z = K$, we can rewrite eq. (11) as

$$H_{\text{intr}} + \frac{\hbar^2 R^2}{2\mathscr{I}} = \frac{\hbar^2}{2\mathscr{I}} [I(I+1) - K^2] + H_{\text{C}} + H_{\text{intr}} + \frac{\hbar^2}{2\mathscr{I}} [\boldsymbol{J}^2 - K^2], \tag{12}$$

where H_{C} is given by eq. (1) apart from the pairing factor, which does not arise in this simple development, and where $j_\pm$ now refers to either particle. The 2-q.p. matrix we diagonalize corresponds exactly to the right side of eq. (12), provided the last two terms make up $E_{\nu 1} + E_{\nu 2}$ from eq. (2) and $(U_1 U_2 + V_1 V_2)$ equals one. For most of our cases the latter of these is nearly true. However, if H_{intr} is held constant, the former is generally not true since states distributed like $(\hbar^2/2\mathscr{I})[\boldsymbol{J}^2 - K^2]$ would cover a range of only around 2 MeV above H_{intr}, with a favoring of high K-values, whereas, $E_{\nu 1} + E_{\nu 2}$ covers a range of around 10 MeV above the gap and the distribution of K-values depends on the position of λ. Thus we do not expect, nor find, our solutions to be very near the limit of complete decoupling.

However, a somewhat surprising situation can occur. The lowest-lying configurations, represented in fig. 4b, do not involve any appreciable high-K components, nor even any with high Ω-values, since both particles must have j nearly parallel to R.

These configurations, therefore, are composed mainly of states where both particles have low Ω, and if λ lies low in the $i_{13/2}$ orbital, these states *will* be spread over a range of 2 MeV, or even less, above the gap energy. Fig. 3 shows this for the lowest three Ω-values and a rather low λ. Thus *for these configurations* eq. (12) is approximately satisfied, with H_{intr} nearly constant and equal to the gap energy, and eqs. (9) and (7) are approximately valid, even though the particles are far from completely decoupled. This result was also found by Vogel [10]) and by Nakai and Kammuri [11]) in the one-

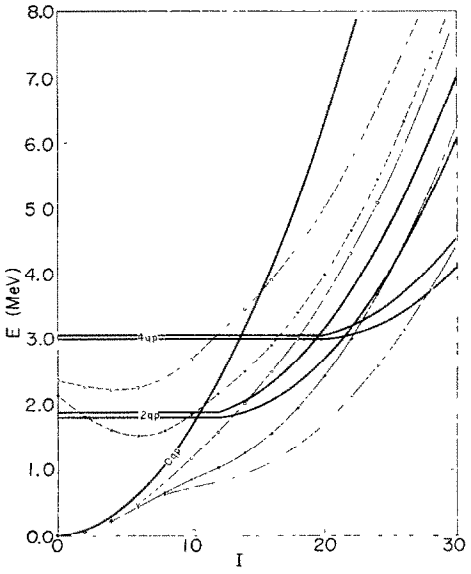

Fig. 6. Excitation energy versus angular momentum for a doubly even rotational nucleus. The heavy lines indicate the lowest two even-spin levels of the completely decoupled system [eq. (9)] for 2q.p. and 4q.p. states, together with the unperturbed ground band (0q.p.). The points and light lines are the lowest (or second-lowest, dashed lines) solutions from the diagonalizations described in subsect. 4.3. The solid points correspond to calculation (a) the open circles to (b) and the crosses to (c).

particle case. At a somewhat more fundamental level this behavior occurs because a few $i_{13/2}$ particles coupled to the maximum J and aligned with R happens to be almost entirely consistent with *both* the Coriolis requirement *and* the requirement of maximum overlap of the particles with the core, provided the core is prolate and the number of particles is not too large. It is perhaps of interest to note that for a few holes in the $i_{13/2}$ orbital the above situation again arises if the core is oblate.

The heavy lines for the 2-q.p. states in fig. 6 correspond to the lowest two values of eq. (9) for even I with $E_0 \approx 1.8$ MeV (see the above paragraph) and $\hbar^2/2\mathscr{I} = 12.5$ keV. The lowest state has $R = 0$, $J = I$ up to $I = 12$ and thereafter $R = I-12$, $J = 12$. The next lowest has $R = 2$ up to $I = 12$ and from there on has $R = I-10$, $J = 10, 12$. This state is twofold degenerate for $I \geqq 12$ and the third lowest state (not

shown) would be threefold degenerate in this spin region, etc. The same development just made for the 2-q.p. states can also be made for the 4-q.p. states, though the approximations are worse. Also, mixing between the 2-q.p. and 4-q.p. states cannot be taken into account in this simple limit. Nevertheless the 4-q.p. energies analogous to those from eq. (9) are plotted as the upper lines in fig. 6, with $E_0 \approx 3.0$ MeV and $\hbar^2/2\mathscr{I} = 10$ keV. The main characteristics are similar to those for the 2-q.p. states except that $R = 0$ can now be extended up to $I = 20$ since $J \leqq 20$. We have also put a line in fig. 6 corresponding to the unmixed ground state band. From these five lines we could draw almost all the main conclusions of sect. 4, but it seems better to do this together with the results of the diagonalizations.

4. Results

Of the results which come out of these calculations at least two are so general that they would be true for almost any perturbing interaction. Since these two are, perhaps, the ones most essential to the experimental observations of sect. 1, we will discuss them first, and later consider the results peculiar to the Coriolis interaction.

4.1. BAND STRUCTURES

In a deformed nucleus where there is a perturbing interaction among a set of levels, and neither the interaction nor the levels change sharply with I, band structures will always develop. By band structures we mean a set of levels, one at each spin value or at least every other spin value, whose energies vary smoothly with spin and which are interconnected by enhanced E2 transitions. These are properties of a rotational band, for instance, but could be more general. They are also the properties needed in sect. 1 to account for the short feeding times and the lack of isomers among the high-spin states. At the most general level, this is perhaps obviously true for a deformed nucleus, since the perturbing interaction will eventually organize a new structure which, if the deformation is retained, can then remain intact as rotational angular momentum is added. Even *while* this new structure is being organized the changes with I may be gradual enough that over a limited region of I an intermediate structure is approximately preserved. One can see this general effect in fig. 6 for the lowest 2-q.p. state above spin 12. This state has, for its internal structure, $J = 12$ and the lowest consistent value for K (not sharp). As I increases this internal structure remains nearly unchanged as rotational angular momentum is added. This is essentially a pure rotational band, and the same is true for the second two degenerate levels which have $J = 10$, lowest K, and $J = 12$, second-lowest K.

It is, however, useful to look in somewhat more detail at this phenomenon. In fig. 7, we indicate the lowest solutions from the matrix diagonalization for spin I, and label them $m = 1$, 2, etc., according to energy. The same is done for spin $I+2$, with n as the labeling index. Our assumption is that the perturbing interaction varies *slowly* with I, so that the *main* difference between the matrices for I and $I+2$ is that the

initial energies of each state differs by the rotational energy, as in eq. (2). Thus the *main* difference in the solutions will be this difference of a rotational energy, which is quite smooth with I. To higher order, if the interaction is increasing with I – the Coriolis interaction is approximately linear with I – then in the energy region of interest the $I+2$ states will be lowered with respect to the I-states, and the mixed band will be compressed in energy compared to the input bands. Since the difference between the I and $I+2$ matrices is small, the lowest solution from I will have a wave function similar to that of the lowest solution of $I+2$, etc. The nature of this wave function depends on the perturbing interaction, but the similarity of the two is more general.

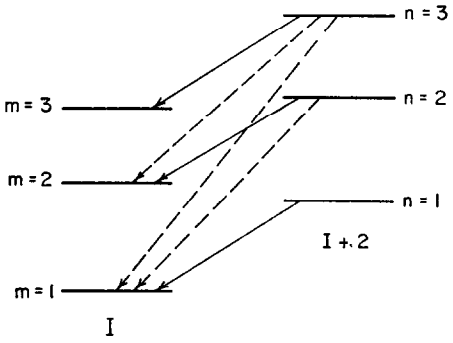

Fig. 7. A schematic illustration of the lowest three solutions for spins I and $I+2$, with some of the interconnecting E2 transitions indicated.

We now consider the B(E2) values between the states indicated in fig. 7. The wave functions for a given solution, $|IM, m\rangle$, can be written

$$|IM, m\rangle = \sum_K a_K^m(I)\phi_K \mathscr{D}^I_{MK}, \tag{13}$$

where the $a_K^m(I)$ are amplitudes, ϕ_K signifies a particular input configuration (0 q.p., 2 q.p., or 4 q.p. in our cases) and the $\mathscr{D}^I_{MK}$ is the usual rotational wave function. (We use K to identify a particular input configuration throughout this paper; though, in fact, more quantum numbers are required. Also, since the Coriolis interaction preserves reflection symmetry about a plane through the origin and perpendicular to the symmetry axis, we take the ϕ_K to be symmetrized in the usual way, involving both positive and negative K-values. Thus the summations here and in eqs. (6) and (7) run over only positive K-values.) The B(E2) value between two such states can be written

$$B(\mathrm{E2}; I+2, n \to I, m) = \sum_{\mu M'} |\langle IM', m|M(\mathrm{E2}, \mu)|I+2\ M, n\rangle|^2, \tag{14}$$

where M(E2, μ) is the usual E2 operator. In evaluating eq. (14) it is clear that the B(E2) values between components ϕ_K and $\phi_{K'}$ are of single-particle strength or smaller unless $K = K'$, in which case they are the enhanced rotational values, $(5/16\pi)Q_0^2$.

Keeping only the enhanced terms gives

$$B(\mathrm{E2}; I+2, n \to I, m) = \frac{5}{16\pi} Q_0^2 [\sum_K \langle I+2K20|I+22IK\rangle a_K^m(I) a_K^n(I+2)]^2. \quad (15)$$

For large I the above Clebsch-Gordan coefficients are virtually independent of K, and approach the limit, $\sqrt{\frac{3}{8}}$. Eq. (15) can then be written

$$B(\mathrm{E2}; I+2, n \to I, m) \approx \frac{3\times 5}{8\times 16\pi} Q_0^2 [\sum_K a_K^m(I) a_K^n(I+2)]^2. \quad (16)$$

The remaining summation in eq. (16) looks like the one occurring in an orthogonality integral, which would be written

$$\sum_K a_K^m(I) a_K^{m'}(I) = \delta_{m,m'}. \quad (17)$$

Since we have argued above that the states n look much like the states m for $n = m$, it follows from eqs. (16) and (17) that

$$B(\mathrm{E2}; I+2, n \to I, m) \approx \frac{15}{128\pi} Q_0^2 \delta_{m,n}; \quad (18)$$

that is, the transitions having solid lines in fig. 7 have the full rotational strength, and those with dashed lines vanish. It is easy to see that transitions of the type $I+2, n \to I+2, n'$ also vanish, since in this approximation the Clebsch-Gordan coefficient again factors out and the sum in eq. (16) now really *is* the orthogonality integral. These are precisely the selection rules needed in sect. 1 to bring the population down in spin very quickly, but keep it spread over several bands.

The B(E2) values according to eq. (15) have been routinely calculated following our Coriolis diagonalizations, and, as examples of the above general rule, the values for those transitions indicated in fig. 7 have been plotted as a function of spin in fig. 8 for one of the 2-q.p. calculations (see subsect. 4.3). The prediction of full rotational strength for $n = m$ is borne out with remarkable accuracy above $I \approx 10$. Below $I \approx 10$ individual 2-q.p. amplitudes become large and cause irregularities, as seen in the $3 \to 3$ and $3 \to 2$ transitions. The transitions for $n \neq m$ all show rather pronounced peaks around $I = 8$ or 10. The reason for this is that the ground band intersects the 2-q.p. bands rather sharply near this spin in this particular calculation (as also happens in fig. 6), and the assumption that the matrices look nearly the same for adjacent spin values is not valid here, particularly relative to the ground band. Thus, at the point where the ground band intersects other bands, not only does the developing energy gap (with decreasing I) favor population of the ground band, but the B(E2) values for this population also peak in just this region. This seems to provide a very general explanation for rather sudden population of the ground band near this point, in accordance with the observations.

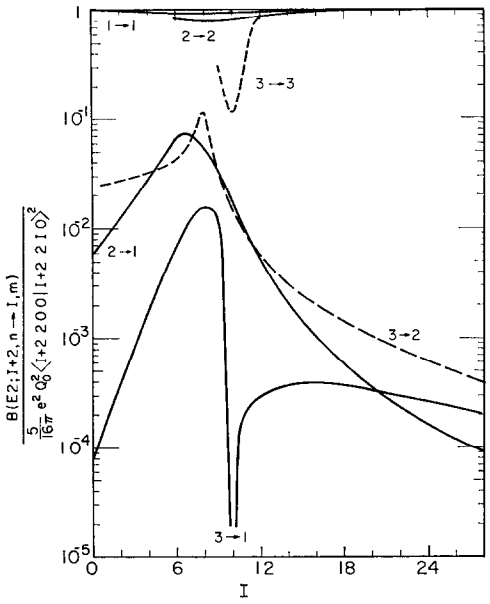

Fig. 8. The $B(E2)$ values (divided by the rotational value with $K = 0$) for the transitions indicated in fig. 7 are plotted as a function of I. The labels refer to $n \to m$ as used in fig. 7, and the values are from calculation (a) described in subsect. 4.3.

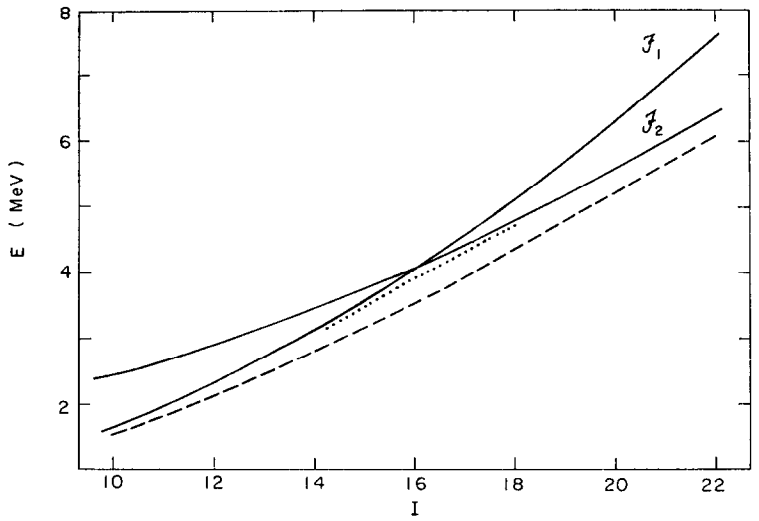

Fig. 9. The solid lines show the energies of two rotational bands as a function of I. The bands have different moments of inertia ($\hbar^2/2\mathscr{I}_1 = 15$ keV, $\hbar^2/2\mathscr{I}_2 = 10$ keV) and are arranged to intersect at $I = 16$. The dotted and dashed lines show the energies of the mixed bands resulting from cases B and C, respectively, in fig. 10.

4.2. ROTATIONAL LEVEL SPACINGS

In this section we want to consider the detailed rotational spacings of the ground band as, for example, have recently been measured by Johnson *et al.* [4]) (see sect. 1). In the general case where the ground band intersects another band, the features of these spacings can be reasonably well characterized. Fig. 9 shows the simplified situation of two bands with constant, but different, moments of inertia around their intersection point at I_C (16 in this case). We want to follow the *lowest* band, and if there is no interaction between the bands we simply change suddenly from one to the other at I_C. When plotted as $\mathcal{I}$ versus ω^2, this makes a discontinuity as shown by the dashed line

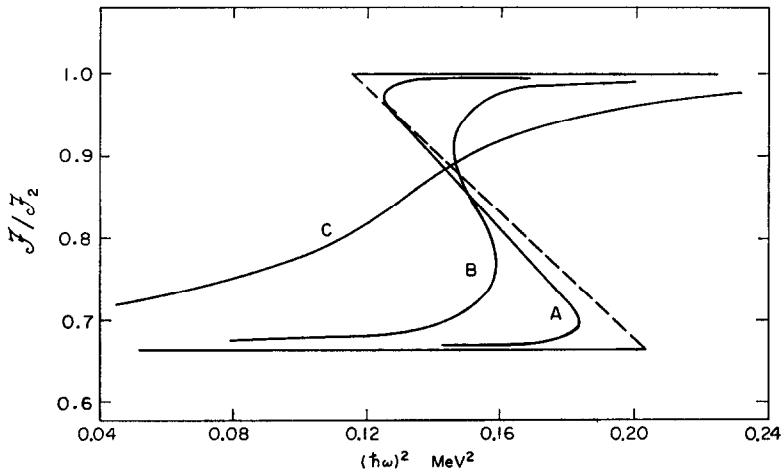

Fig. 10. The ratio $\mathcal{I}/\mathcal{I}_2$ is plotted versus ω^2 for the lower band in fig. 9. The horizontal lines connected by a dashed line correspond to no mixing between the bands, C corresponds to inter-band matrix elements comparable to the maximum g.s.b.-2q.p. ones used in our calculations, B to matrix elements 3 times smaller, and A to ones 10 times smaller. We have used $\mathcal{I} \propto (4I-2)/(E_I-E_{I-2})$ and $\hbar\omega \approx 2(I-1)\,(E_I-E_{I-2})/(4I-2)$, which differ slightly from those others have used, but not enough to affect this or fig. 15 significantly.

in fig. 10. This discontinuity causes lower values of ω^2 above I_C if $\mathcal{I}_2/\mathcal{I}_1 > (I_C+2)/I_C$. This might generally be the case around $I = 20$ since $(I_C+2)/I_C$ is then only ≈ 1.1. As an interaction is introduced between the bands, the discontinuity is rounded, first into an S-shaped curve like A in fig. 10, and then with increasing interaction, like B and finally C. This range covers the observed behaviour, those of Johnson *et al.* being of the S-shaped variety (A or B in fig. 10), whereas most previously measured ones appear to be more like C. Thus, in the present framework, the occurrence of S-shaped curves depends on two factors: (i) the difference between the effective moments of inertia of the two bands at their intersection point, which determines the transition to be made and (ii) the strength of the interaction between the bands which determines how sharply this transition is made. In subsect. 4.3 it will be seen that the present Coriolis calculations give shapes covering the full range of fig. 10.

4.3. RESULTS OF STANDARD CORIOLIS CALCULATIONS

In this section we will present the results of our Coriolis diagonalizations for three "standard" sets of conditions. These were chosen to be the best *a priori* estimates we could make for the input parameters. The main emphasis of this section will be on an attempt to understand the origin of the effects produced in these diagonalizations, rather than on trying to fit any particular experimental feature. The effects of variation of the input parameters will be discussed in subsect. 4.4, again with mainly the above emphasis. The first standard calculation (a) included only the ground band, 0-q.p., and 2-q.p. bands. The 2-q.p. states included all those from the $i_{\frac{13}{2}}$ orbital as given by Nilsson at $\eta = 6$. The Fermi surface was placed midway between the $\Omega = \frac{3}{2}$ and $\frac{5}{2}$ states ($\approx$ 94 neutrons), and Δ was taken to be 0.9 MeV. The $\hbar^2/2\mathscr{I}$ values were set at 15.0, 15.0 and 12.5 keV for the 0-q.p., 0–2-q.p., and 2-q.p. states respectively. This variation was made in an attempt to take into account the reduction of the pairing correlations in the 2-q.p. states. The $\langle\Omega\pm1|j_\pm|\Omega\rangle$ values were calculated from the Nilsson wave functions. These data, together with eqs. (1)–(5), defined the input information. For the second standard calculation (b) the only change was to raise λ to a point between the $\Omega = \frac{7}{2}$ and $\frac{9}{2}$ states ($\approx$ 104 neutrons). The third calculation (c) was like (a) except that only $\Omega = \frac{1}{2}$–$\frac{7}{2}$ states were included, but then all possible 4-q.p. states were generated. The Δ(2 q.p.–4 q.p.) was taken to be 0.6 MeV and the 2–4-q.p. and 4-q.p. values for $\hbar^2/2\mathscr{I}$ were taken to be 12.5 and 10.0 keV, respectively. The results of these three calculations will now be summarized.

The energies of the lowest two states from calculations (a) and (b), and the lowest state from calculation (c) have been plotted in fig. 6. Perhaps most remarkable here is the agreement of the lowest 2-q.p. state (the lowest state above $I \approx 12$) from (a) with the completely decoupled limit for this state, $|(12, I-12)IM\rangle$. We have commented in sect. 3 that this is due to the fact that mainly only low-Ω components are required for this lowest state, and these lie low in the 2-q.p. spectrum of (a). When these states are raised to higher energies in (b) the special favoring of this state ends, and its agreement with the limit is virtually destroyed. Above $I = 12$, the second lowest state in (a) is considerably higher in energy than its limit, $|(12, I-10)IM\rangle$, consistent with the fact that eq. (6) shows $|(12, I-10)IM\rangle$ to involve much larger high-K admixtures than does $|(12, I-12)IM\rangle$. A consequence of this is that there is always a large gap between the lowest and second lowest states whenever the Fermi surface is low, as in (a). In calculation (b) there is no especially favored state and the energy gap between the lowest and second-lowest state is smaller, and, under some conditions, essentially vanishes.

The inclusion of 4-q.p. states has reasonably little effect below $I \approx 20$. Fig. 6 shows that the lowest state in (c) is pushed lower in energy due to the addition of 4-q.p. states ($\approx$ 0.7 MeV at $I = 20$), but up to spin 20 or so this is not a large fraction of the total lowering of the 2-q.p. states due to the Coriolis interaction (about 5 MeV at $I = 20$). A separate calculation including only $\Omega = \frac{1}{2}$–$\frac{7}{2}$ and 0-q.p. and 2-q.p. states gave energies very similar to (a) in fig. 6, so that the difference between (a) and (c) *is*

probably due mostly to the addition of 4-q.p. states, and hopefully contains most of that effect. We can calculate the relative importance of the number of quasiparticles in the yrast state according to

$$F_i(I) = \sum_K a_{iK}^2(I), \qquad i = 0, 2, 4, \tag{18}$$

where the $a_{iK}(I)$ are the amplitudes of the configuration K, with i quasiparticles, in the yrast state of spin I. Fig. 11 shows the $F_i(I)$ for calculation (c), and they look

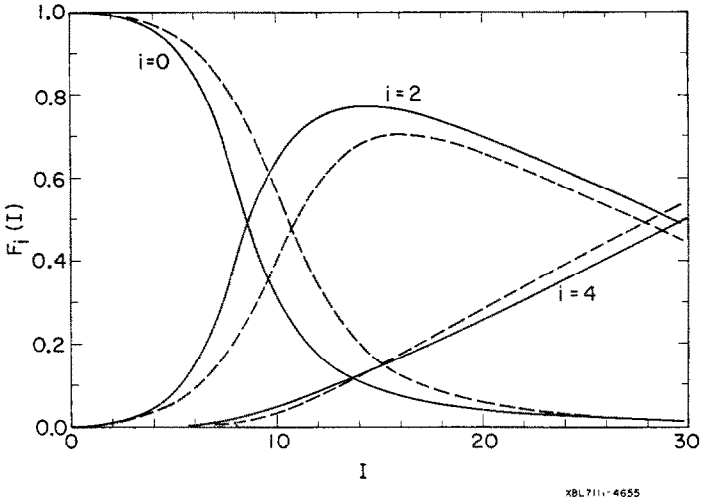

Fig. 11. The $F_i(I)$ [eq. (18)] are plotted versus I for calculation (c). The dashed line shows the effect of the reduced pairing factor [eq. (20)].

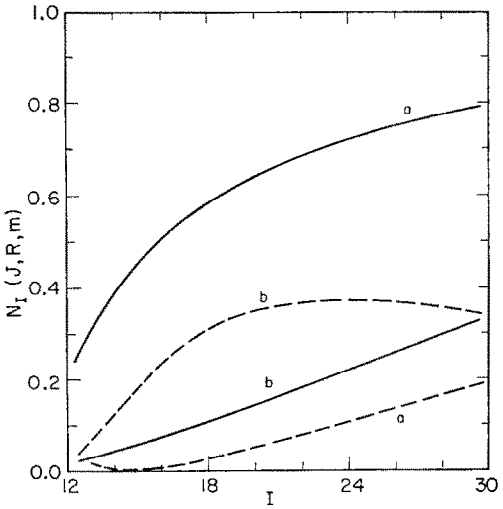

Fig. 12. The $N_I(J, R, m)$ values [eq. (19)] plotted against I. The solid lines correspond to $N_I(12, I-12, 1)$ and the dashed lines to $N_I(12, I-10, 2)$ with a and b indicating calculation (a) and (b). It should be noted that the $N_I(J, R, m)$ are the squares of overlap integrals.

much as one would guess from the limiting lines in fig. 6. The 2-q.p. configurations dominate the yrast state from the ground-band crossing, $I \approx 10$, until $I \approx 30$. This should not be taken too seriously, but it probably *does* suggest that in the crucial region for us, $I = 10$–20 it is reasonable to make calculations with only 0- and 2-q.p. states, provided one is not looking at fine details. This is important since (c) already contains 55 states (1 0-q.p., 16 2-q.p. and 38 4-q.p.) and only about half of the $i_{\frac{13}{2}}$ orbital.

To test the degree to which our wave functions correspond to those configurations given in eqs. (6) and (particularly) (7), we can form the square of the overlap:

$$N_I(J, R, m) = \langle (JR)IM | IM, m\rangle^2, \tag{19}$$

where the $|(JR)IM\rangle$ are defined in eq. (6), and the $|IM, m\rangle$ in eq. (13). In fig. 12 we plot the $N_I(12, I-12, 1)$ for calculations (a) and (b), (c) is not possible since the set of input configurations is not complete. These overlaps are more or less what one would expect from the energies in fig. 6: in (a) the configuration $|(12, I-12)IM\rangle$ is rather pure above $I = 20$ or so, but in (b) it is still developing at $I = 30$. We also show $N_I(12, I-10, 2)$ in fig. 12, and it is apparent that this state is much more poorly developed than the lower-energy one in (a), but comparably or better developed in (b). At lower spins individual 2-q.p. configurations can still be important, and cause large irregularities in the curves; so fig. 12 was not extended into this region. Even above $I = 12$, other overlaps can be important. The most notable example is the configuration, $|(10, I-10)IM\rangle$, in the lowest state of calculation (b), where its overlap exceeds the one plotted for all spin values. The competition of these three configurations in the lowest two states of (b) is rather strong, and leads to the decline observed in $N_I(12, I-10, 2)$ at the highest spin values. In spite of such intriguing features, the overall pattern implied by fig. 12 is unmistakable, and conforms with the discussion in sect. 3.

The problem of the B(E2) values has been discussed in subsect. 4.1 in connection with the band structures which develop. It is interesting that the band characteristics, as indicated by the B(E2) values and energies of figs. 8 and 6, are much better developed than the overlaps of fig. 12 might suggest. To understand whether the level system generated here really can account for the observed feeding patterns of the g.s.b., we assumed equal population in all levels at $I = 30$ and followed this decay down in spin, taking account of the B(E2) values [eq. (15), fig. 8] and the fifth-power energy dependence of E2 transitions. The population pattern is shown in fig. 13 for the three lowest states of calculation (a). The agreement of that for the lowest state with the observed patterns (sect. 1) is reasonably good, although perhaps the calculated feeding is not quite sharp enough. This pattern, including the spin at which the population enters the lowest level, is reasonably sensitive to the Coriolis strength, the position of λ, and the $\hbar^2/2\mathscr{I}$ values (see subsect. 4.4). It may also be true that when other systems of levels are considered, (i) the odd-spin values, (ii) other orbitals for one or both neutrons and (iii) protons in various orbitals, then the feeding pattern could be modified to

some extent (see subsect. 4.5). Nevertheless, provided E2 transitions dominate the de-excitation, the overall situation shown in fig. 13 looks quite encouraging to us.

It is important to see if the feeding times estimated from these calculations are in agreement with those observed. This cannot be the case for (a) and (c), since fig. 6 shows that cascades along the yrast levels between $I = 10$ and 20 involve several transitions that have less energy than 300 keV. The E2 lifetimes are very sensitive to energy, and there is no way transitions of this (or lower) energy can be involved in feeding times around 10 psec. However, we know that such energies do not occur at these spins in nuclei of the type we are considering, so that we could not expect these

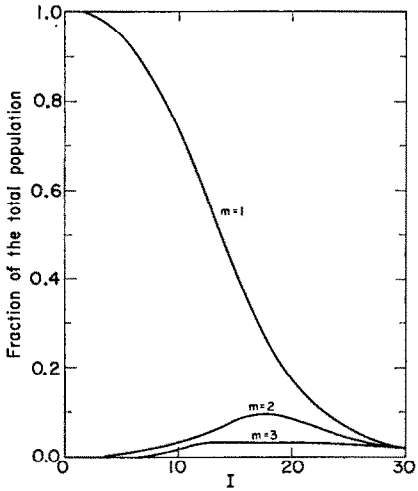

Fig. 13. The fraction of the total population found in the lowest three states is plotted as a function of I for calculation (a).

cases to lead to reasonable feeding times. Curve (b) looks more like real nuclei in this respect, though the transition energies in this spin region are still low. We have not yet calculated the feeding times, but can estimate them as follows. We include the five lowest levels at each spin value, and compute the mean lifetime of each (considering only these E2 transitions). We then weight each level according to the population it receives in that calculation, and compute a weighted-average lifetime for each spin value. These we sum down to spin 10 (arbitrarily) and call this the mean feeding time (of the $I = 10$ state). For curve (b) this turns out to be 15 psec. It is perhaps interesting to note that if we continue down in spin in this case, we find a 10 μsec $I = K = 8$ isomeric state populated to the extent of 4 %. If we reproduce the experimental energies, then the feeding times get shorter. For the "realistic" case considered at the end of subsect. 4.4, the feeding time is 5 psec, and the 50 individual levels involved in this estimate had lifetimes ranging from 0.02 to 6 psec. The behavior of these feeding times seems to be very regular as the general arguments in subsect. 4.1 suggest. If the cal-

culations are adjusted to give the known transition energies, they appear to give feeding times in the correct range.

In this discussion we have not considered odd-spin states nor the possibility of M1 transitions playing a significant role in the de-excitation. It is easy to show that M1 transitions vanish in the limit of complete decoupling. The allowed M1 selection rules are: $R = R'$ and, since for our case no odd J-values exist, $J = J'$. A section of the level scheme given by eq. (9) is shown in fig. 14. It is apparent that all allowed M1 transitions have no energy. In our diagonalizations the odd-spin states do tend to lie near or even above the next-higher even-spin states, so that the allowed M1 transitions

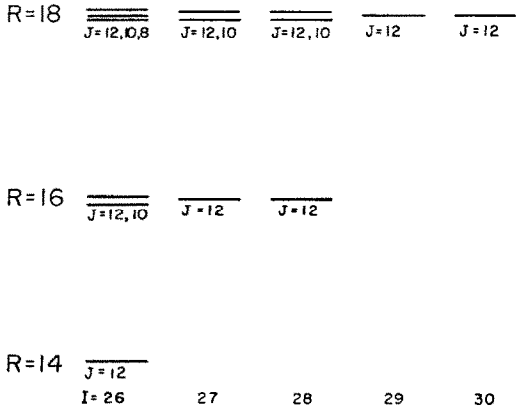

Fig. 14. A section of the completely decoupled level scheme given by eq. (9).

do not seem likely to compete with the E2 transitions. However, the forbidden, or "hindered", M1 transitions of the type M1($I+1$, $n \rightarrow Im$) have more and more energy available as n becomes large compared with m; and to know if (or where) they compete with the E2 transitions requires a detailed calculation of the amount of their "hindrance". These calculations we have not yet made, so the question cannot be answered at present. Conceivably, transitions of this type could define the energy "width" of the yrast cascade.

The plots of $\mathscr{I}$ versus $(\hbar\omega)^2$ for the three calculations are given in the top portion of fig. 15 (see subsect. 4.2). The S-shape is rather pronounced for (a) and (c) due mainly to the fact that the ground state band intersects the 2-q.p. states in a region where they are almost completely flat with energy ($\mathscr{I}_{\text{eff}} \approx \infty$). This behavior is reasonably sensitive to the input parameters (see subsect. 4.4), and thus may not occur, but it points out the fact that in the Coriolis framework the apparent moment of inertia of the yrast band can be temporarily larger than the rigid-body value. As an example where this happens, it is known that in 2-q.p. doubly odd nuclei, values of twice $\mathscr{I}_{\text{rig}}$ occur [12]). The dramatic effect of varying λ is shown in the results for calculation (b). This occurs mainly because the Coriolis effects in the 2-q.p. states are much smaller, resulting in a lowest 2-q.p. level that rises sooner and more strongly than in (a) or (c).

This in turn results in a later intersection with the g.s.b. and a smaller change in $\mathscr{I}$ at that point. Even in this case the effect comes at a value of $(\hbar\omega)^2$ considerably lower than that observed, ≈ 0.08 MeV^2. Lowering the Coriolis effects by reducing $f(U, V)$ [eq. (1)] for the 2-q.p. states has rather large effects as discussed in subsect. 4.4. These detailed calculations seem to bear out the general arguments made in subsect. 4.2.

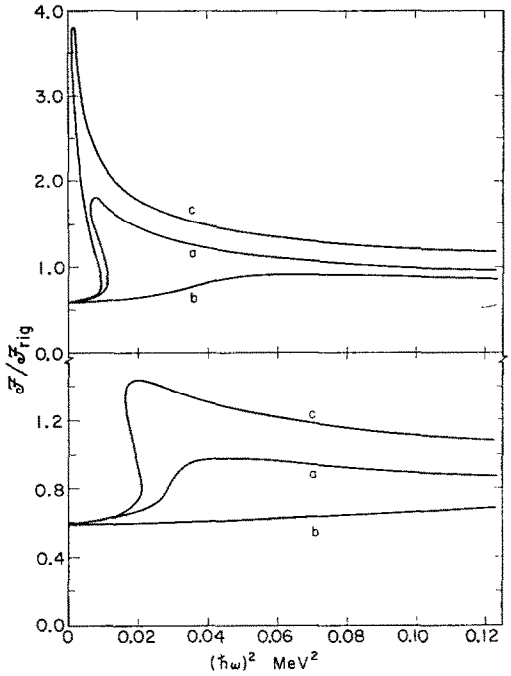

Fig. 15. Plots of $\mathscr{I}/\mathscr{I}_{rig}$ versus $(\hbar\omega)^2$ (see caption to fig. 10). The upper set of curves is for the three "standard" calculations, and the lower set has the $f(U, V)$ given in eq. (20).

An interesting point is that *these* Coriolis calculations do not produce large distortions in the rotational spacings at low spin values. We put in $I(I+1)$ spacings for the g.s.b., and usually find in the results a value around 3.3 for ratio of the energies of the 4^+ to 2^+ states, no matter how dramatic the distortions become at larger I. If effects of this type are to account for the energy deviations at low I, many additional levels must be involved and this situation is probably better treated by the usual Coriolis-antipairing calculations. This conclusion does not seem to us inconsistent with the present idea that the intersection of the g.s.b. with other levels *at higher spin values* may nevertheless involve primarily a limited group of levels. Also, other effects, like centrifugal stretching, are undoubtedly involved to some extent in the ground-band energy deviations.

4.4. THE VARIATION OF INPUT PARAMETERS

In this section we will discuss briefly how the results presented above vary with the input parameters, Δ, $\hbar^2/2\mathscr{I}$, λ and $f(U, V)$. It is easy to see that Δ is not very important. From the decoupled limits shown in fig. 6, one can see that sliding the 2-q.p. and/or 4-q.p. states up or down by rather large amounts has rather little effect – perhaps changing the 0–2-q.p. and/or 2–4-q.p. intersection points by $2\hbar$ or so. Also the effect of Δ on $f(U, V)$ is not large and, for the 2- and 4-q.p. states, there is a compensating effect on the energy level separations. Thus, varying Δ within reasonable limits has little effect on the results.

Variation of the $\hbar^2/2\mathscr{I}$ values makes considerably larger effects on the results, though not so large as one might at first think. The higher energies of the 2-q.p. and 4-q.p. input states [eq. (2)] for a larger $\hbar^2/2\mathscr{I}$ are compensated (in the levels of interest) by increased Coriolis matrix elements [eq. (1)], which, in the calculation, lower these input energies by a larger amount. In the limiting case in fig. 6, one sees that there is no residual effect at all of $\hbar^2/2\mathscr{I}$ on the lowest 2-q.p. energies up to $I = 12$ and the lowest 4-q.p. energies up to $I = 20$. In the detailed calculations the 2- and 4-q.p. states have a tendency for lower energies at low spins and higher energies at high spins for larger values of $\hbar^2/2\mathscr{I}$. The first of these tendencies together with the larger ground-band spacings produces an intersection point at lower spin values for larger $\hbar^2/2\mathscr{I}$. If, for example, all $\hbar^2/2\mathscr{I}$ values are 20 keV then the intersection point between $I = 8$ and 10 (amplitude of g.s.b. = 0.7) in calculation (a) drops to between $I = 6$ and 8. This trend is in general accord with the observation that more-vibrational nuclei are populated at lower spins, but both these intersection points seem too low for the $\hbar^2/2\mathscr{I}$ values involved. This can be taken as one of many indications that the Coriolis effects are too large in these *a priori* estimates.

We have already remarked on the surprisingly large effect of varying λ, and the reasons for this (subsect. 4.3). This is undoubtedly the reason why Coriolis effects in neutron states of the rare-earth region are larger than those in proton states, and it is tempting to wonder whether it is not somehow related to the much greater apparent "softness" of the neutron-deficient rare-earth rotors as compared with the neutron-rich ones. The reduction in the Coriolis effects with higher values for λ suggests that feeding points for (HI, xn) reactions should be higher for the heavier (or neutron-richer) rare-earth nuclei and also that the irregularities in the yrast level spacings should come later and be smaller. A careful study of these points might constitute a test of these ideas.

There is evidence from the odd-mass nuclei that the Coriolis strength in these high-j orbitals is reduced more than the simple estimate we use in eq. (4). Specifically the odd-mass data indicate that the Coriolis matrix elements connecting states across the Fermi-surface are around half that expected, whereas those connecting states either well above or below the Fermi-surface are not reduced. We can reproduce just this type of behavior if we rewrite the upper portion of eq. (4) as

$$f(U, V) = (U_1 U_2 + V_1 V_2)^5, \tag{20}$$

but we should emphasize that this is just an *ad hoc* empirical factor that gives the correct general features. All our calculations have been repeated with this modification, and the results are much more reasonable than those discussed above. The energies of all the lowest mixed levels are higher, crudely by around 0.04 I MeV, and all the effects we have described take place at higher spin values, as indicated by the g.s.b.-2-q.p. crossing in fig. 11. Surprisingly, the overlaps with the decoupled limit, the $N_I(J, R, m)$ values, shown in fig. 12 are all larger for $I \gtrapprox 20$; the largest one is only a few percent larger, but the lower three are nearly doubled. The largest change is in the $\mathscr{J}$ versus ω^2 plots, and we show this effect for the three calculations in fig. 15b. Not only are the shapes more like those observed, but the intersection occurs at larger values of $(\hbar\omega)^2$, which is better in accord with the experimental data, though still not high enough. The energy separation of the lowest two mixed states is also substantially reduced by eq. (20) in the cases we have examined, particularly in case (b). It seems to us that the reduction of eq. (20) gives a clear improvement in the results, and still larger reductions are indicated.

A related point concerns the 0–2-q.p. matrix elements, the lower part of eq. (4). The $f(U, V)$ factors for this case range from ≈ 0.5 when both states are near the Fermi surface to nearly zero when both lie far above or below this point. There is no experimental evidence, as far as we know, from the odd-mass nuclei which bears on this question, so we really do not know how accurate these values are likely to be. It is interesting to note that while the $\mathscr{J}$ versus ω^2 plots are rather sensitive to this coupling strength, the intersection point of the g.s.b. and 2-q.p. levels is quite insensitive to it, as is the behavior of the levels at higher spin values.

We have not yet explored the problem of fitting these calculations to the detailed experimental data. Although a careful study of this does not seem warranted at the present time, it is important to know whether, in a general way, this model can account for the observed features with reasonable variation of the parameters. Most specific in the experimental data are the $\mathscr{J}/\mathscr{J}_{\text{rig}}$ versus $(\hbar\omega)^2$ plots of Johnson *et al.*, and we chose the λ-values of calculations (a) and (c) more or less to represent these nuclei. Since the 4-q.p. states seem to be more important than the high Ω-values, we begin with calculation (c) using the modification of eq. (20). The $\mathscr{J}/\mathscr{J}_{\text{rig}}$ versus $(\hbar\omega)^2$ curve for this calculation is plotted in the lower part of fig. 15, and when compared with the data: (i) the transition occurs at too low a value for I, (ii) also at too low a value of $(\hbar\omega)^2$ and (iii) the amplitude of the effect is too large. All these indicate that the Coriolis effects are too large, and all are corrected as well as could be desired, without going to a particular nucleus, by multiplying all non-diagonal matrix elements by 0.7. The resulting curve does not quite bend back at the transition point, but rather small variations in the 0–2-q.p. matrix elements change this behavior rather dramatically without affecting much else. The only feature not easily reproduced is the slope of the experimental curves prior to the transition, at low $(\hbar\omega)^2$, as discussed at the end of subsect. 4.3. The feeding pattern, fig. 13, also looks better, in that the lowest level is more sharply fed around $I = 16$, and the estimated feeding time of 5 psec is most

reasonable. It appears to us that the model *can* fit the data provided such reductions of the Coriolis strength are considered reasonable. Conversely, if one believes the model, rather specific information about the Coriolis interactions can be obtained. But it seems to us premature to make very much of either of these points at the present time.

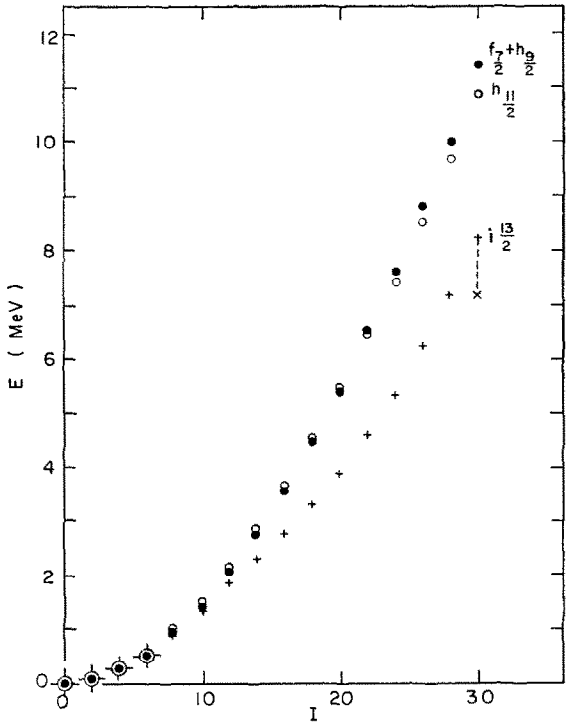

Fig. 16. The energy of the lowest solution from systems of "core plus two particles" is plotted versus I. The two particles are placed in the $f_{\frac{7}{2}}$ plus $h_{\frac{9}{2}}$, the $h_{\frac{11}{2}}$, or the $i_{\frac{13}{2}}$ orbitals. The effect of using eq. (4) instead of eq. (20) is shown on the $I = 30$ point of the $i_{\frac{13}{2}}$ case, and would be rather similar for the other orbitals.

4.5. THE EFFECT OF OTHER j-SHELLS

We have argued in sect. 2 that the Coriolis effects in the $i_{\frac{13}{2}}$ orbital are much larger than in other orbitals at a given spin value. We can test this within the framework of the present calculations by comparing the results for the $i_{\frac{13}{2}}$ orbital that we have discussed above with those we would get by taking other orbitals to treat explicitly. The yrast energies that result from the $h_{\frac{9}{2}}$ plus $f_{\frac{7}{2}}$ neutron orbitals and the $h_{\frac{11}{2}}$ proton orbital are compared with those from the $i_{\frac{13}{2}}$ neutron orbital in fig. 16. In all cases Nilsson wave functions[8]) at $\eta = 6$ were used. The λ-value corresponded to calculation (a) for

the neutron levels, and was placed at the $\Omega = \frac{7}{2}$ level (Ho isotopes) in the $h_{\frac{11}{2}}$ proton shell. The other conditions were approximately those of calculation (a) except that eq. (20) was used. The $i_{\frac{13}{2}}$ states lie considerably lower than the others at high spin values, confirming our expectations. Also, as the $i_{\frac{13}{2}}$ particles decouple, the angular momentum carried by the rotation of the core is reduced (ultimately by 12 $\hbar$), thereby inhibiting the decoupling in the other shells. In fact, decoupling a *second* pair of particles in one of these other orbitals might be rather like decoupling a *second* pair of $i_{\frac{13}{2}}$ particles – calculation (c) – and hence of major importance only for $I \approx 30$.

We also need to consider the effect of these other orbitals on the de-excitation process. For simplicity we will consider the negative-parity orbitals in the 82–126 shell as one group since they are admixed together by the deformation. It would not change the present arguments essentially if they were broken down into smaller groups. If there are two particles in these negative-parity orbitals then the lowest level of this system is shown (approximately) on fig. 16 as the $f_{\frac{7}{2}}$ plus $h_{\frac{9}{2}}$ curve and the de-excitation would feed into the g.s.b. in much the same way as in the case of the $i_{\frac{13}{2}}$ system, except that the g.s.b. might already contain admixtures from the $i_{\frac{13}{2}}$ 2-q.p. states at this feeding point. If these two systems mix heavily enough, the de-excitation of the upper one to the lower one might occur at considerably higher spins. A more interesting case is that of one particle in the $i_{\frac{13}{2}}$ orbital, and one in the negative-parity orbitals. The lowest level of this negative-parity system probably lies between the $i_{\frac{13}{2}}$ and the $f_{\frac{7}{2}}$ plus $h_{\frac{9}{2}}$ curves in fig. 16. The population in this system can decay at each spin either by E1 transitions to the lower $i_{\frac{13}{2}}$ system (or to the g.s.b. at low spin) or by collective E2 transitions to base of the negative-parity system. In the latter case an isomer results, but of the spin and K-value of the base, or lowest-lying, member of this system. Such "low" spin isomers *are* sometimes observed following (HI, xn) reactions [13]). The competition between the E1 and E2 transitions, which relates to the amount of population going into these isomers, depends on the location of λ, among other factors, and simple estimates only show that it cannot be easily predicted. For example, a 1 MeV E1 transition of 10^{-4} single-particle units seems reasonable to expect, and should just begin to compete with the E2 transitions. The protons, in our view, would behave in a similar fashion. We can see nothing in this picture that would conflict with the experimental situation outlined in sect. 1, though we have not made calculations beyond those shown in fig. 16.

5. Conclusions

In the previous sections we have considered the direct Coriolis effects on particles in various j-shells, principally the $i_{\frac{13}{2}}$ shell, in a rotational nucleus, and found the following properties. At moderately high values of the spin ($I \gtrapprox 10$) a pair of these particles tend to decouple from the core and align their angular momenta, $2j-1$, with the rotational angular momentum of the core. This state, whether fully decoupled or not, lies very low in the two-quasiparticle spectrum and generally intersects the rising

ground state band somewhere between $I = 10$ and 20. Thus, our calculations suggest that the lowest-lying band changes character rather abruptly in this region to one where two particles, $i_{13/2}$ particles in the beginning of the rare-earth deformed region, are (or tend to be) decoupled from the core. If the Coriolis matrix elements are somewhat reduced over the *a priori* estimate, this picture fits rather well the experimental data on rotational spacings and feeding following (HI, xn) reactions. This method for carrying angular momentum with the minimum expenditure of energy combines that used by the deformed nuclei for lower spin values – rotation – with that used by the near-closed-shell nuclei – aligning high-j particles – and suggests that, at least in some cases, the combination is more efficient than either one separately.

The picture we have presented ignores any other significant changes that may be occurring in the nucleus as the angular momentum increases. It does not seem so likely that such other changes will totally prevent or submerge the tendencies of the Coriolis interaction, but they may certainly interrupt, delay, or temporarily overshadow them. The Mottelson-Valatin effect might represent an example of such a change. This is the phase transition caused by the Coriolis force from the state with pairing correlations to the one without, and is expected to occur rather suddenly at around $I = 20$. This effect is not the same as the decoupling that we are discussing, though both are related in that they have a common cause, the Coriolis force. In our model the pairing correlations are reduced in the yrast levels only by the increase in the number of quasiparticles in this state (fig. 11) and, if at some point they vanish, it would be because for that number of quasiparticles they were never present. In our terminology, the Mottelson-Valatin effect would be an indirect effect of the Coriolis force, and is not included in our calculations because it is neither in our input spectrum nor in the Coriolis matrix elements. In fact, the two phenomena are based on a rather different assumption. We have argued that, due to favorable circumstances (sect. 2), the $i_{13/2}$ orbital will react to the Coriolis force at much lower spin values than the other proton or neutron orbitals. For the Mottelson-Valatin effect, however, the Coriolis force evokes a coherent response from *all* orbitals at the same spin. To do this there would presumably have to be some inhibition of the Coriolis effects in the highest-j orbitals and an enhancement in the lowest-j ones. A rather large inhibition in the $i_{13/2}$ orbital would indeed seem to be necessary to delay the decoupling if it is not occurring before $I = 20$. Whether such reductions of the Coriolis matrix elements occur or not is currently an open question. For high-j orbitals in odd-A nuclei there seems to be a reduction of about a factor of two over what one expects in the immediate vicinity of the Fermi surface, but none at higher quasiparticle energies (see subsect. 4.4). Reductions somewhat larger than this are necessary in the 2-q.p. system just to delay the decoupling to a reasonable spin value (≈ 16). The experimental picture is not yet very clear for the lower-j orbitals. If the decoupling is prevented around $I = 16$ by such coherent effects, it would nevertheless seem to us that the tendency to decouple would again be strong in the nucleus after the phase transition. Changes in the shape of the nucleus might represent another class of "interruptions" of the decoupling process.

In conclusion, there now seems to be experimental evidence building up that a major change occurs in the rotational levels of rare-earth nuclei around $I = 16$. There is a long-standing prediction that such a rather sudden change would occur as a result of the loss of the pairing correlations. The present work suggests that the decoupling of a pair of particles can give a second possible explanation for such a change. It now seems to be an interesting and challenging problem to find ways to determine which, if either, of these explanations is correct.

We are indebted to many people for discussions and comments on various aspects of this problem. Among these are: S. Bjørnholm, J. de Boer, R. M. Diamond, T. Kammuri, P. Kienle, H. J. Mang, B. R. Mottelson, K. Nakai and S. G. Nilsson. We thank Mr. R. J. Lutter for his help with the computer program. The encouragement and support of Prof. J. de Boer and the Sektion Physik der Universität München is gratefully acknowledged.

References

1) J. O. Newton, F. S. Stephens, R. M. Diamond, W. H. Kelly and D. Ward, Nucl. Phys. **A141** (1970) 631
2) J. R. Grover, Phys. Rev. **157** (1967) 832;
J. R. Grover and J. Gilat, Phys. Rev. **157** (1967) 862; *ibid* 814; *ibid* 823
3) B. R. Mottelson, The Nuclear Structure Symp. of the Thousand Lakes, Joutsa, Finland, August 1970; Fifth Nordic-Dutch Accelerator Symposium, Ebeltoft, Denmark, May 1971
4) A. Johnson, H. Ryde and J. Sztarkier, Phys. Lett. **34B** (1971) 605
5) B. R. Mottelson and J. G. Valatin, Phys. Rev. Lett. **5** (1960) 511
6) R. M. Diamond, G. Symons, J. Quebert, K. Nakai, K. H. Maier, J. Leigh and F. S. Stephens, Nucl. Phys., submitted
7) K. A. Hagemann, S. A. Hjorth, H. Ryde and H. Ohlsson, Phys. Lett. **28B** (1969) 513
8) S. G. Nilsson, Mat. Fys. Medd. Dan. Vid. Selsk. **29** (1955) no. 16
9) K.-G. Rensfelt, A. Johnson and S. A. Hjorth, Nucl. Phys. **A156** (1970) 529;
J. Alonso, H. Bakhru, F. M. Bernthal, J. Boutet, B. Olsen, I. Resanka and J. O. Rasmussen, Nucl. Phys., submitted;
R. M. Diamond, J. R. Leigh and F. S. Stephens, unpublished data
10) P. Vogel, Phys. Lett. **33B** (1970) 400
11) K. Nakai and T. Kammuri, private communication, March, 1971
12) J. R. Leigh, F. S. Stephens and R. M. Diamond, Nucl. Phys. **33B** (1970) 410
13) J. Burde, R. M. Diamond and F. S. Stephens, Nucl. Phys. **85** (1966) 481